Multidisciplinary non-invasive investigations to develop a hydrogeological conceptual model supporting slope kinematics at Fontana Cornia landslide, Northern Apennines, Italy

Multidisciplinary non-invasive investigations to develop a hydrogeological conceptual model supporting slope kinematics at Fontana Cornia landslide, Northern Apennines, Italy

Alessandro Aguzzoli[1] · Diego Arosio[1] · Marco Mulas[1] · Giuseppe Ciccarese[1] · Benedikt Bayer[2] · Gerfried Winkler[3] · Francesco Ronchetti[1]

Abstract
A multidisciplinary approach focusing on the integration of diverse and non-invasive investigations is presented to define the hydrogeological conceptual model of the complex Fontana Cornia landslide in the Northern Apennines, Italy. The results of seismic refraction tomography and electrical resistivity tomography investigations indicate that the landslide has a cur-vilinear sliding surface dividing the shallow calcarenite debris layer from the deeper pelitic bedrock. The surface presents undulations in which water can be stored and supports the application of the fill and spill hypothesis that is seldom used in landslide studies. The joint interpretation of the geophysical outcomes and of the hydrogeological and hydro-chemical analy-ses of a spring located on the slope allows the definition of the landslide hydrogeological conceptual model. Four specific hydrologic stages with different groundwater flows though the landslide body were identified. The developed hydrogeological model may explain the displacements of the landslide that were detected with In-SAR monitoring. The isotopes analyses, the displacement monitoring, and the hydrogeological measurements confirm that periods with significant precipitations and snowmelt can cause an increase in landslide saturation that in turn triggers larger displacements. Conversely, the landslide slowly moves at a steady rate during periods with limited recharge water.

Keywords Landslide · Geophysical methods · Fill and spill hypothesis · Environmental isotopes · In-SAR · Hydrochemistry

Introduction

It is well known that groundwater plays a key role in determining the kinematic and dynamic behaviour of unstable slopes (Bogaard and Greco 2016; Sidle et al. 2019; Ivanov et al. 2020). The hydraulic features of the landslide media, their spatial distribution as well as their surface and subsurface geometries strongly control water infiltration, degree of saturation, pore water pressure distribution and groundwater circulation. As a consequence, detailed knowledge of the slope hydrogeological features, the landslide geometry and of the lithological boundaries is of major importance for engineers and geologists dealing with landslide risk management. Several studies addressing unstable slopes have focused on investigations and analyses aimed at the definition of comprehensive hydrogeological conceptual models (e.g., Krzeminska et al. 2012; Vallet et al. 2015). Unfortunately, the harsh and uneven conditions of the slopes, including fractures, trenches, scarps, deep gullies and sparse rock boulders, often make in-depth and extensive field investigation activities difficult to be performed at reasonable costs. For these grounds, non-invasive techniques, including geophysical, hydrogeological and remote sensing methodologies, have been increasingly used for landslide assessment and monitoring, especially by employing portable and flexible equipment (Cappa et al. 2004; Corsini et al. 2015a). With respect to conventional geotechnical investigations (e.g., boreholes), geophysical surveys are able to analyse large areas in a non-destructive manner and processed geophysical data can supply reliable information about geo-mechanical, geo-electrical and geometric subsurface features (Jongmans

Diego Arosio
diego.arosio@unimore.it

1 Dipartimento di Scienze Chimiche e Geologiche, Università degli Studi di Modena e Reggio Emilia, Modena, Italy

2 Fragile S.r.l., Bologna, Italy

3 Institut für Erdwissenschaften, Universität Graz, Graz, Austria

and Garambois 2007). Common outcomes of landslide geophysical investigations include compressional- and shear-wave velocity maps, depth to water table, bedrock or slip surfaces, networks of major discontinuities, preferential pathways and areas for water circulation and storage, amplification and polarisation phenomena related to the slope stability conditions (Meric et al. 2005; Longoni et al. 2012; Mainsant et al. 2012; Del Gaudio et al. 2013; Arosio et al. 2019; Taruselli et al. 2020; Aguzzoli et al. 2021). Though almost all geophysical techniques, both active and passive, have been employed for landslide characterisation, seismic and electrical methods are generally preferred because their outputs are strongly related to the geomechanical properties and to the water content of the landslide materials that in turn control the overall slope stability.

As far as hydrogeological analyses are concerned, when no deep groundwater investigations can be undertaken, i.e. boreholes with water level monitoring, non-invasive methods can be nevertheless employed to identify hydraulic processes in both fractured-rock and porous-medium aquifers (Maloszewski et al. 1992; Birk et al. 2004; Glynn and Plummer 2005; Tazioli et al. 2012; Winkler et al. 2016; Ronchetti et al. 2020; Wagner et al. 2020). The general approach in landslide hydrogeology usually involves spring discharge monitoring coupled with hydro-chemical assessment. Several authors have applied physical and chemical monitoring of springs to investigate recharge processes, water storage characteristics, groundwater flow rates and transit times in both fractured and porous aquifers (Deiana et al. 2017; Brkić et al. 2018).

This study presents a multidisciplinary approach dealing with the integration of diverse non-invasive investigations that were performed to define the hydrogeological conceptual model of the compound (Delgado et al. 2011) Fontana Cornia landslide (FCL). Despite the harsh environment, geophysical techniques were employed to identify the geometry of the subsurface layers along with hydrogeological and chemical monitoring of a spring inside the FCL to define the groundwater subsurface flow features. The geophysical surveys were performed chiefly to support the interpretation of the hydrogeological, hydro-chemical and remote sensing datasets in the framework of the FSH. Moreover, the metric and decametric calcarenite blocks scattered over the landslide surface can be used as natural reflectors for the Interferometric Synthetic Aperture Radar (In-SAR) technique. The In-SAR technique allows monitoring the displacement of the blocks over time to study landslide kinematics and any seasonal displacement trends. The innovative fill and spill hypothesis (FSH; Tromp-Van Meerveld and McDonnell 2006) is used to integrate the diverse pieces of information obtained from the previous methods and to support the definition of the slope hydrogeological conceptual model. The integrated interpretation in the framework of the FSH aims at linking the slope hydrogeological conceptual model to the kinematics of the landslide and may be a useful tool to understand the evolution of landslides.

Background geology and climate

The study area is located in the northern Apennines, Italy, on the South-East flank of the Epiligurian calcarenite slab referred to as Pietra di Bismantova (Fig. 1a). It belongs to the Appennino Tosco-Emiliano National Park and it is an important site from both naturalistic and touristic points of view (Borgatti and Tosatti 2010). The slab covers an area of about 1.5 km^2, has a maximum elevation of 1041 m a.s.l. and is bordered by 100 m-high vertical walls crossed by steeply dipping fractures (Fig. 1b). The slab consists of calcareous sandstone with several crack sets having different attitudes that decrease the stability of rock pillars and walls. In late 2014, a crackmeter monitoring network was installed on potentially unstable rock elements (Corsini et al. 2016) and, in winter 2015, the collapse of a 200 m^3 block was observed (Mulas et al. 2020). Since then, some seismic noise measurement sessions have been also carried out on blocks that are believed to be unstable (Arosio et al. 2017).

The top of the calcarenite slab can be approximated with a sub-horizontal plane slightly dipping to the west. Underneath the calcarenite layer, there are Ligurian pelitic formations (Papani et al. 2002) consisting of impermeable fine material composed of marls with thin volcanoclastic layers. The pelitic formations outcrop as gently dipping slopes (from 10 to 30°) surrounding the slab. The arcuate eastern section of the slab is lower (945 m a.s.l.) and thinner and it is affected by a lateral spreading phenomenon that evolves downslope into a roto-translative SE-trending deep-seated landslide (Fig. 1a). The combination of the above-mentioned phenomena results in the compound FCL. These mass movements involve metric blocks detached from the calcarenite slab that downslope fragment into debris (Fig. 1c). The landslide is about 0.8 km long and its toe reaches *Casale* village (Fig. 1a).

Water can infiltrate into the calcarenite slab only through the wide fractures on the top because of its massive compact nature with extremely low permeability. The pelitic formations are also classified as an impermeable lithology (Gargini et al. 2008; Tazioli et al. 2019). Consequently, water infiltrates into the landslide body through voids produced by the toppling and the roto-translative movements of the calcarenite blocks and debris. To identify the main hydrogeological features of the investigated area, a spring located within the landslide body at an elevation of about 800 m a.s.l. was monitored (Fig. 1a).

The area has a rainy, hot temperate climate with wet summers. The mean annual rainfall over the last 70 years has

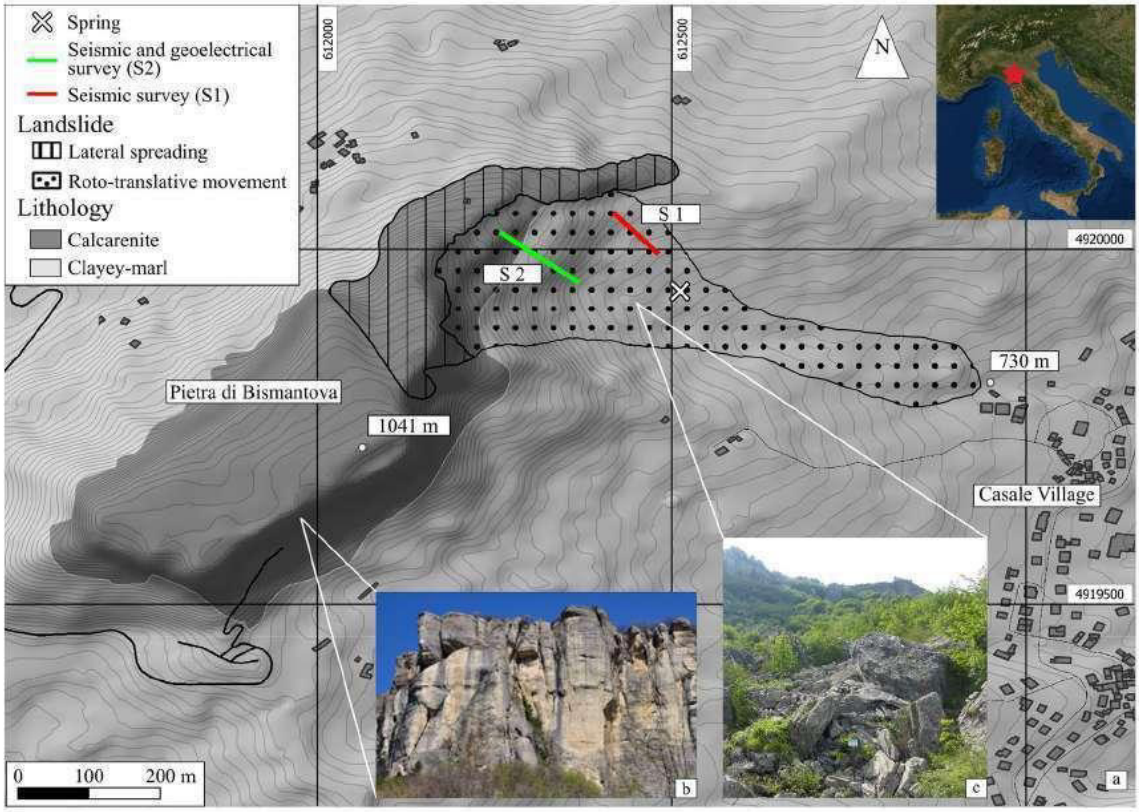

Fig. 1 **a** Geological setting of the Fontana Cornia Landslide; **b** SE-facing walls bordering the Pietra di Bismantova; **c** calcarenite blocks outcrop-ping in the roto-translative section of the landslide

been of approximately 900 mm. More precisely, the yearly precipitation distribution has two main peaks: a first one in autumn and another one during the spring season. Generally, evapotranspiration is higher during late spring and summer (from May to September) and snow can accumulate at the surface from November to March.

Several technologies spanning from in situ to remote sensing can be used to monitor surface displacement in active landslides (Corsini et al. 2015b; Thiebes et al. 2016; Liu et al. 2018). In particular, In-SAR techniques have undergone a very significant development in the last decades and are now routinely used to remotely monitor slow-moving landslides, especially where numerous natural reflectors (e.g., outcropping rocks) are located on the investigated slope (Iasio et al. 2012; Bayer et al. 2018).

The surface of FCL is characterised by the presence of outcropping rock blocks ranging from 0.01 to 5 m^3 that work as reflectors for the application of the multi-temporal satellite interferometry, consisting in the analysis of numerous interferograms to solve millimetric displacements over time for pixels with high coherence. In detail, 134 ascending and 127 descending Sentinel-1 radar scenes were processed using the small baseline implementation of the Stanford Method for Persistent Scatterers (StaMPS; Hooper et al. 2007). The mean velocity estimated along the satellite line of sight (LOS) for the ascending and descending orbits (Figs. 2a and b, respectively) shows that higher values (5–30 mm/year) are clustered in the middle and upper sections of the landslide. Figure 3a, b depict the mean cumulated LOS displacement and velocity of selected points enclosed into the red and blue contours in Fig. 2a, b, respectively. Some of these reflectors are located around the monitored spring.

The maximum cumulative displacement is 37 mm, giving an average LOS velocity of 12.3 mm per year. However, two acceleration events can be observed, the first one in May–June 2016 and the second one in February 2018, both after intense snow falls (Fig. 3c) and the following snow melt.

Methods

Geophysical site investigation

Two seismic surveys to study the subsurface geometries within the landslide body were performed. The first spread (November, 2018) was placed close to the north-eastern border of the landslide (hereafter S1; Fig. 4a) to study the

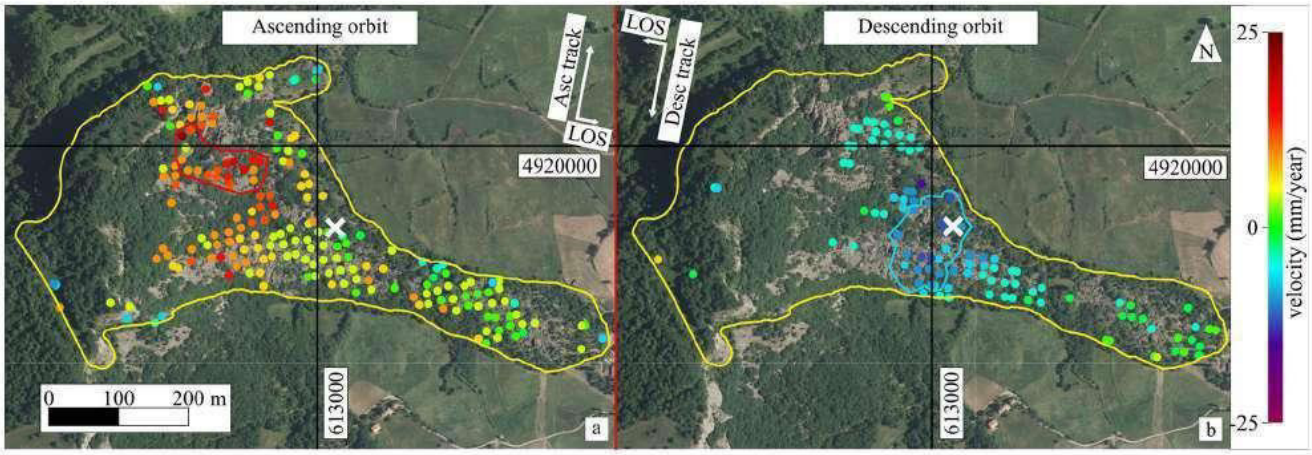

Fig. 2 Multi-temporal In-SAR results for ascending (**a**) and descending (**b**) orbits. Points enclosed into the red and blue contours were selected to estimate LOS displacement and velocity depicted in Figs. 3a, b, respectively. The yellow contour represents the landslide outline, and the white cross indicates the spring

debris cover and the underlying pelitic layer. Here, layers are believed to have smoother and more regular geometry and the sliding surface is assumed to be shallow. The second spread (February, 2019) was deployed along the slope dip direction (hereafter S2; Fig. 4) to investigate the subsurface structures related to rock pillars and boulders detached from the main calcarenite slab as a consequence of the above-mentioned lateral spreading phenomenon.

Two Geometrics Geode (https :// www. geome trics. com/) systems were used to collect seismic data from 48 GeoSpace vertical geophones with a natural frequency of 4.5 Hz. Geo-phones had a spacing of 2 m and of 3 m for S1 and S2, respectively. Several in-line shots were fired both out and within the spreads according to a reciprocal configuration to collect data that could be processed with P-wave refraction tomography or employing the standard reciprocal methods. For S1, a buffalo gun was used, while for S2 an 8 kg sledge-hammer was preferred because of the presence of debris at the surface that could not grant effectively confined shots for the buffalo gun. However, the performance of the sledge-hammer has been proved to be comparable to the one of the buffalo gun in similar conditions (Zhang et al. 2020). At some locations in the top section of S2, geophones were mounted on heavy bases to achieve a satisfactory coupling because of big boulders outcropping. Accurate locations of sources and sensors were determined by means of a dif-ferential global navigation satellite system (GNSS) survey.

Recorded seismic data were processed according to the seismic refraction tomography (Sheehan et al. 2005) by using PyGimli, an open-source python library designed for modelling and inversion in geophysical problems (Rücker et al. 2016). The inversion scheme involves error-weighted minimisation through the Gauss–Newton method (Loke et al. 2003) and works with unstructured meshes. The regularisation parameter λ is also used to control the rough-ness of the inversion by weighting the spatial derivatives of the velocity model. The input data are the first arrivals that were manually picked whenever the signal-to-noise ratio (SNR) was considered satisfactory. As a matter of fact, shots fired in the lower half of S2 were more effective and first arrivals could be generally picked on all the receivers. An initial velocity model was set with a vertical gradient of 70 m/s per meter on an unstructured 2D mesh optimised by

the software, a wide range of λ was tested and a Chi^2 value equal to 1 was set as stopping criterion to avoid overfitting and indicating that input data were optimally fitted consider-ing the picking errors. As an additional stopping criterion, the maximum number of iterations was set equal to 20.

To limit the ambiguity in the interpretation of seismic data as well as to better relate geophysical outcomes to hydrogeological investigations, an electrical resistivity tomography (ERT; Binley and Kemna 2005) survey was carried out by coupling 48 electrodes to the geophones of S2, except for the above-mentioned outcrops, where no electrode could be planted. To collect the geoelectrical data, the Syscal Pro Switch resistivity meter from IRIS instruments (http:// www. iris- instr uments. com/ syscal- pro. html) was used. Acquisitions were performed with the Wenner-alpha con-figuration because of higher SNR (low geometric factor) and good vertical resolution with respect to other electrode configurations. In addition, a threshold value of 50 mV was set for the voltage difference measured at the potential elec-trodes. The minimum and maximum currents were 3.55 and 63.2 mA, respectively.

2D inversion of the resistivity pseudo-section was again carried out with the PyGimli library with parameters similar to the ones described above, but a homogeneous initial model was set using the median of the measured apparent

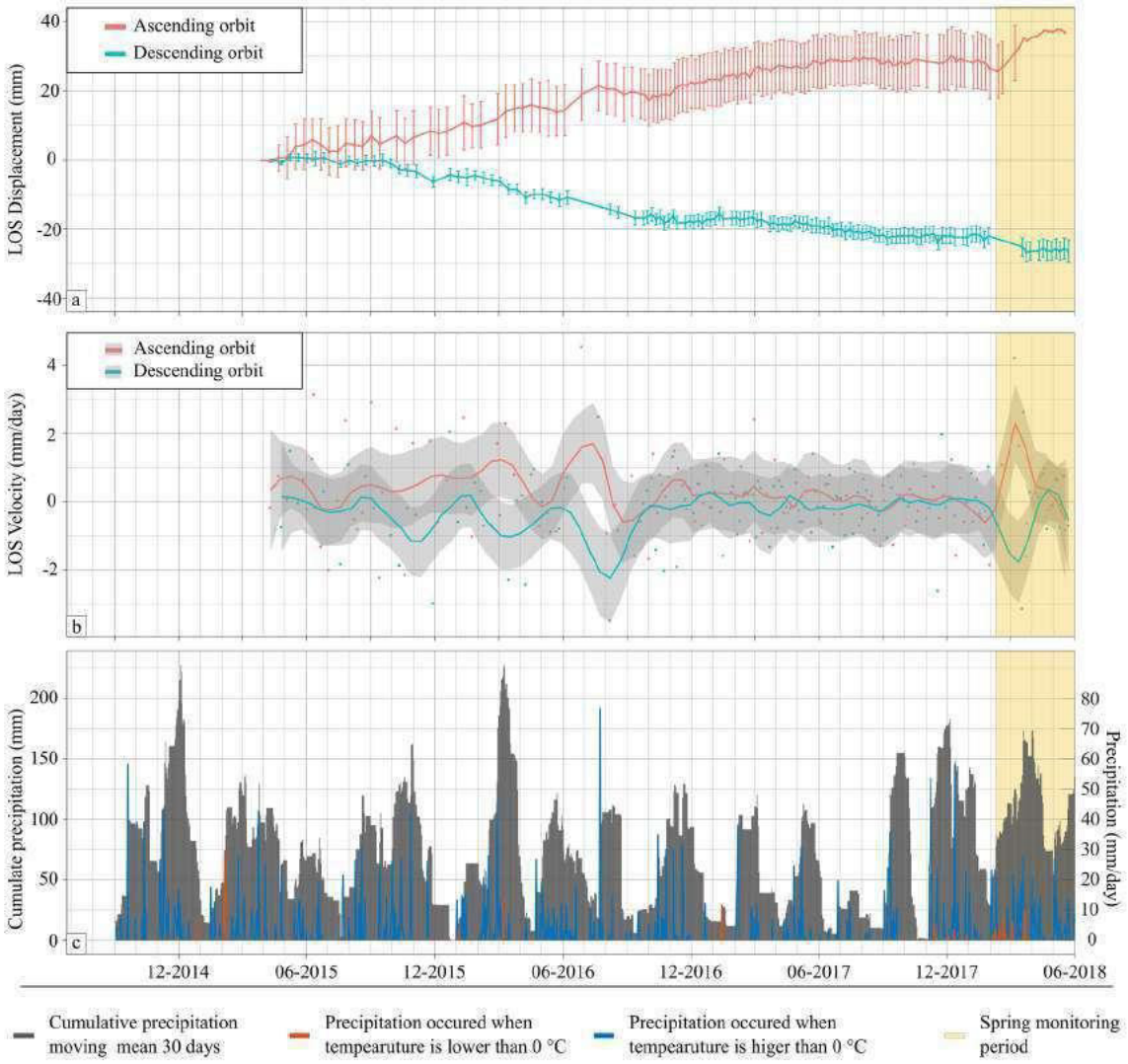

Fig. 3 LOS displacement (**a**) and velocity (**b**) time series retrieved by multi-temporal In-SAR for ascending and descending datasets. Lines in (b) represent LOS velocity obtained by a polynomial regression of the instantaneous velocity. Bars in **a** and grey-shaded areas in **b** indi-cate the standard deviation and the 95% confidence interval, respec-tively. **c** Presents the comparison between the moving mean of the cumulative precipitation computed over 30 days (grey bars), the daily precipitation that occurred when the temperature eas higher than 0 °C (blue line) and the daily precipitation that occurred when the temperature was lower than 0 °C (red line). The yellow rectangle indicates the monitoring period considered in this study

resistivity values and model extent and cell size were defined according to considerations about penetration depth and res-olution as expressed in Roy and Apparao (1971) and Friedel (2003), respectively.

Hydrogeological and hydro-chemical investigations

Physical and geochemical monitoring of spring param-eters and isotope analysis of rainfalls cover the period from 14/02/2018 to 13/07/2018 with different sampling frequen-cies (Fig. 5). The discharge (Q) of the spring (Fig. 1a) was measured using the volumetric method and the natural water electric conductivity (EC) with the portable multiprobe Crison MM40+ . Spring water and snow were sampled on site, while rainfall samples were collected at the Montecagno rainfall gauge (Deiana et al. 2018), approximately 11 km SW of FCL.

The spring water samples were analysed to estimate the anionic concentration using Visocolor colorimetric kits, and the cationic concentration with an inductively coupled plasma-atomic absorption spectrometry (ICO-AES) mass spectrometer (Perkin Elmer Optima 4200 DV, https://www.perkinelmer.com/it/). The absolute values of the ion concen-trations were expressed in ppm and then normalised. The ion concentrations of some specific samples were plotted with the Piper diagram.

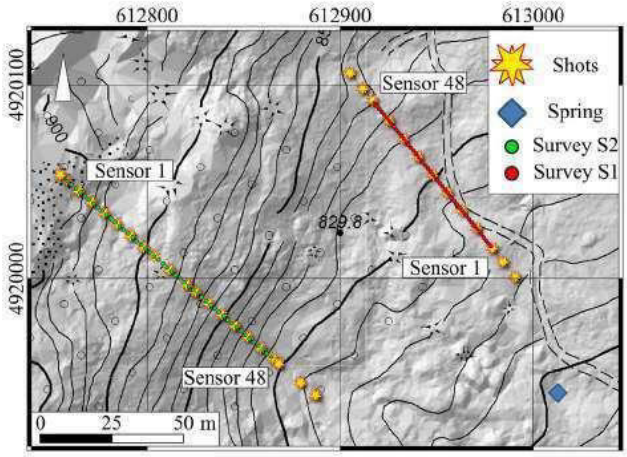

Fig.4 Location of sources and sensors for spreads S1 and S2 on the landslide surface. Yellow stars indicate where shots were fired, the blue square marks the spring location, and points indicate where sensors were deployed. More in detail, red points concern the survey S1, and green points refer to the survey S2

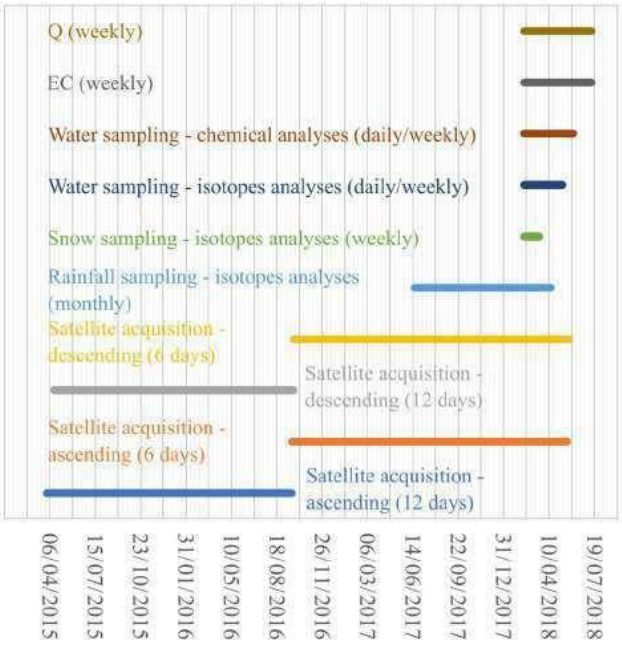

Fig. 5 Hydrogeological and remote sensing monitoring data used in this study with the associated sampling intervals. Q and EC represent the discharge recorded at the spring and the electrical conductivity of the water samples, respectively

Moreover, spring, rain and snow water samples were analysed to estimate the isotopic concentration of oxygen ($\delta^{18}O$) and deuterium ($\delta^{2}H$) in ‰. In more detail, the $\delta^{18}O$ analyses were done using a mass spectrometer and the CO^2 water equilibration technique (Epstein and Mayeda 1953), while the $\delta^{2}H$ analyses were executed using a Los Gatos Research Liquid Water Isotope Analyser 24d (Berman et al. 2009). The analytical errors were 0.10 and 1.0‰ for $\delta^{18}O$ and $\delta^{2}H$, respectively. The results were reported as differ-ences between the sample and the standard (Vienna Standard Mean Oceanic Water; V-SMOW).

Fill and spill hypothesis

The fill and spill hypothesis is commonly used to verify the presence of subsurface morphological undulations in which water can be stored after precipitation events, especially in the presence of lithologies with very low permeability. This method was successfully applied to gently dipping stable slopes (Tromp-Van Meerveld and McDonnell 2006) and rock glaciers (Wagner et al. 2020).

A rainfall event causes the water to infiltrate into the sub-surface and, after a certain time span, water flows out of a downslope spring producing a discharge peak. A recharge event (R) represents the sum of the millimetres of precipita-tion (P) that produce a discharge peak, with V being the total volume of water that flowed out of a spring during the dis-charge peak. The FSH relates R values to V ones providing information regarding the behaviour of the groundwater flow and the geological setting of the investigated site according to the relation:

$$V = k * R, \quad (1)$$

where k is simply the angular coefficient that relates R to V.

Figures 6 and 7 illustrate how two different and originally dry geological settings, without and with undulations at the top of the deeper low-permeability layer, respectively (Figs. 6a and 7a), affect groundwater flows and discharge peaks triggered by different recharge events ($R\square$, $R\bigcirc$, $R\Diamond$, R^* in Figs. 6c and 7d). When no undulations are present, recharge water can directly flow to the spring (Fig. 6b); therefore, all the points in the R–V plane belongs to a line L through the origin (Fig. 6d).

On the contrary, morphological depressions at the top of the low-permeability layer allow recharge water to be temporarily stored in the subsurface (Fig. 7b). As a consequence, groundwater can flow to the spring producing a discharge peak only when undulations have been completely filled (Fig. 7c). According to subsurface conditions, recharge events may generate points in the R–V plane that: (1) lay on the R axis in case recharge water is not enough to fill the undulations (R□); (2) belong to a line m through the origin when subsurface undulations are already saturated (R◇, R*); 3) belong to a line n parallel to line m when part of the recharge water is needed to fill the undulations (Fig. 7e).

Point I represents the intersection between the line n and the R axis and indicates the amount of recharge water needed to fill the undulations. The value of I is not constant and depends

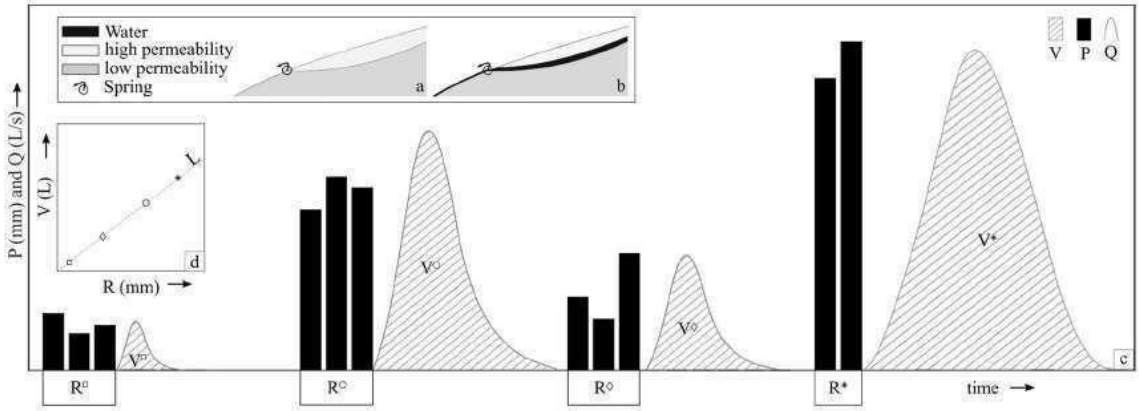

Fig. 6 Dry (**a**) and saturated (**b**) conditions of the subsurface when there are no undulations at the top of the lower impermeable layer. Spring response (V(square), V(circle), V(diamond), V(asterisk)) to different recharge events (R(square), R(circle), R(diamond), R(asterisk)) (**c**). Black bars indicate that the precipitations (*P*) occurred during a certain amount of time and *Q* is the spring discharge. Recorded *R* and *V* values belong to the line L that indicates the expected spring response after a recharge event **d**

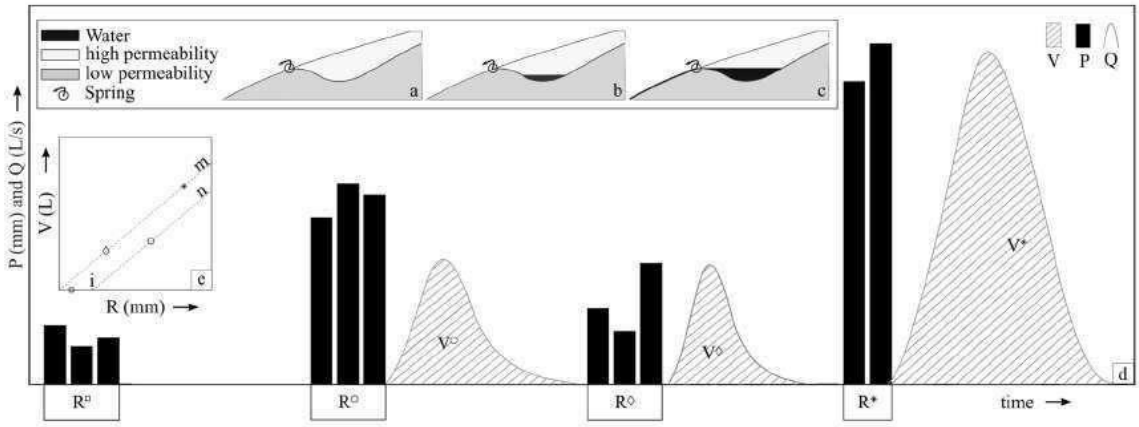

Fig. 7 Three different saturation conditions of the subsurface when there is an undulation at the top of the lower impermeable layer (**a**–**c**). Spring response (V(circle), V(diamond), V(asterisk)) to different recharge events (R(square), R(circle), R(diamond), R(asterisk)) (**d**). Black bars indicate the precipitations (*P*) occurred during a certain amount of time and *Q* is the spring discharge. Recorded *R* and *V* values belong to the line m when the subsurface is saturated and to line n when the undulation is not completely filled. The intersection between line *n* and the *R* axis indicates the water needed to completely fill the undulation (**e**)

on the saturation of the undulation before the occurrence of any recharge event.

The application of the FSH to estimate *k*, *I* and the saturation of the involved media is useful to develop the FCL hydrogeological conceptual model and helps to verify the presence of subsurface undulations where water can be stored.

Results

Geophysical surveys

The result of the seismic refraction tomography concerning S1 approximately shows two layers with different velocities (Fig. 8a). The P-wave velocity (*V*p) is lower than 1000 m/s from the topographic surface to roughly 10 m depth, then *V*p abruptly increases to about 1500 m/s and rises gradually until 3000 m/s, with differences between the sides and the centre of the spread. Lower velocities at the top of the deeper layer may be representative of the altered pelitic bedrock that becomes massive at depth. Also, the seismic section concerning S2 (Fig. 8b) suggests a two-layer structure, though with more marked lateral variations. The P-waves propagate inside the shallow layer with a velocity lower than about 1100 m/s, while the deeper layer has *V*p spanning from 1500 to 3000 m/s. It can be noticed that the boundary between the two layers has a curvilinear trend and becomes shallower moving

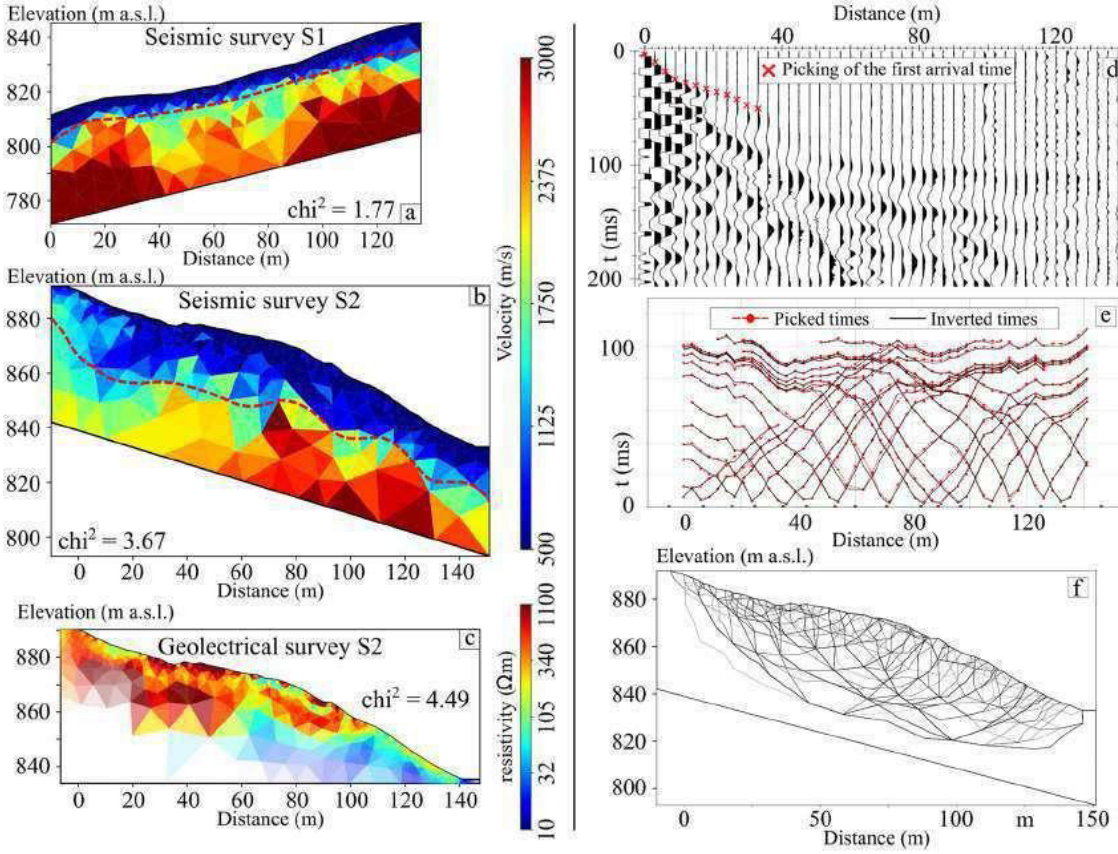

Fig. 8 Seismic refraction tomography results for S1 (**a**) and S2 (**b**), and the ERT section for S2 (**c**). Red dashed lines in (**a**) and (**b**) indi-cate the interface between the top calcarenite debris layer and the deeper pelitic bedrock. Cell transparency in (**c**) indicates the sensitiv-ity of the geoelectrical analysis: the higher the transparency, the lower is the sensitivity. Chi^2 values for each inversion are also reported. Example of seismic record with picking of first arrivals for a shot fired 5 m upslope of sensor 1 of S2 (**d**). Comparison between picked and inverted travel times for S2 (**e**) and the seismic rays associated with inverted travel times (**f**)

downslope. Considering that S2 is a 141 m-long spread deployed in a landslide area and that sources were fired with a sledgehammer, it may be challenging to obtain seis-mic traces at far offsets with SNR high enough to reliably pick first arrivals (Fig. 8d). Figure 8e, f depicts the results of the refraction tomography inversion process for S2 and indicate a good match between picked and inverted travel times.

The ERT results for S2 are in agreement with the seis-mic ones. The resistivity section reported in Fig. 8c again shows a two-layer subsurface, with higher resistivity val-ues (higher than 200 Ωm) for the shallow weathered layer. The transparency of the cells is inversely proportional to the sensitivity of the geoelectrical analysis. The interface between the layers is similar to the one observed in the seismic section except for the toe of the survey where the shallow resistive layer is only a few metres deep. For sake of completeness, we report that all inversions stopped after 20 iterations.

Hydrogeological, hydro-chemical monitoring and fill and spill hypothesis

Results of spring monitoring shows that Q is maximum (4.5 L/s) in late March 2018 in the wet period and minimum (null discharge) in the dry period, while EC presents maxi-mum values in the dry period and minimum values in March (Fig. 9i). As expected, higher rainfalls are recorded during the wet period (February–March and May) and the maxi-mum amount of snow occurs during the colder period of the year (between February and March).

Groundwater chemical analysis shows that the major ions are carbonate and sulphate (Figs. 9a–f) with negligi-ble and significant correlation with EC, respectively (R^2 0.3 and 0.73). Since the sulphate ion is useful to distin-guish lithologies in sedimentary environments, Fig. 9b presents the regression line for all the collected values and the regression line for the two periods considered the most significant for the analysis of the sulphate ion,

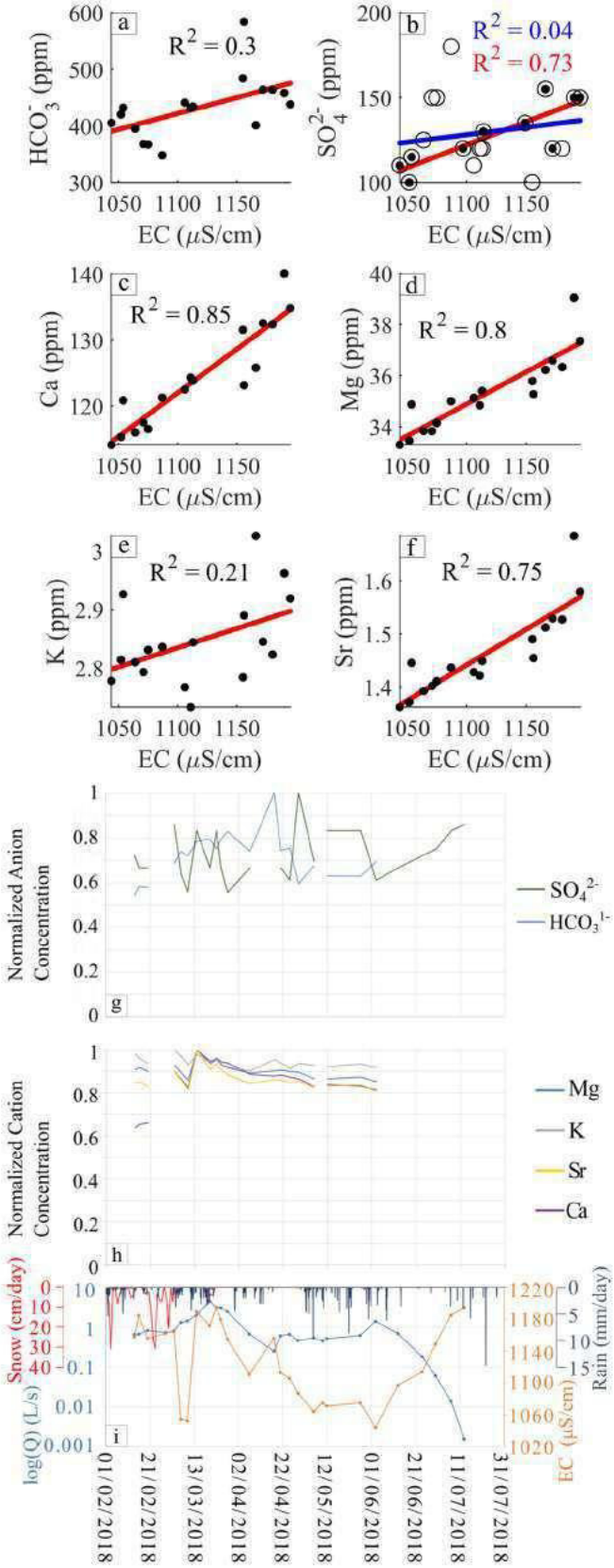

Fig. 9 Concentration of different ions versus EC with tentative regression lines (in red) and the associated R^2 values (**a**), (**b**), (**c**), (**d**), (**e**), (**f**). Please note the different ranges of the y axes. In (**b**), the blue line represents the regression of all values collected in 2018, while the red line is the regression for the two most significant periods, namely the discharge increasing limb recorded during March and the discharge decreasing limb at the beginning of June. Comparison between the normalised anionic (**g**) and cationic (**h**) concentrations resulting from the chemical analyses conducted on spring water samples and (**i**) results of the physical and rainfall monitoring. Plots (**g**), (**h**) and (**i**) share the same x-axis

namely the discharge increasing limb recorded during March and the discharge decreasing limb at the beginning of June. In more detail, sulphate and carbonate ion contents roughly have opposite trends during the monitoring period (Fig. 9g) and EC seems to be occasionally correlated with carbonate ion (e.g., during April; Figs. 9g and i). The analysed cations, Ca^{++}, Mg^{++}, K^{+}, and Sr^{++} with calcium being the main one, show the same trend during the monitoring period (Fig. 9h) with different correlations with EC values (R^2 0.85, 0.8, 0.21 and 0.75, respectively; Figs. 9c to f). All the collected groundwater samples highlight a Ca–HCO_3 affinity that can be due to the interaction between water and calcarenite blocks and debris. Values measured in February are not shown in Figs. 9c, d, e and f because they are believed to be related to a previous recharge period. However, these points are shown in Fig. 9h because the monitoring period started on February 14th.

The Piper diagram (Fig. 10a) provides the percentage of the ion concentrations of some specific samples and shows that sulphate ions occasionally replace carbonate ions, with the former having higher concentrations in the dry period (July) and the latter in the wet one (April). Finally, analyses performed to investigate $\delta^{18}O$ and $\delta^{2}H$ isotopes (Fig. 10b) show all samples are aligned along the local meteoric line (NIMWL; Longinelli and Selmo, 2003). Isotopic data of snow present ranges between − 96.8 and − 169.9 ‰ for $\delta^{2}H$ and between − 13.4 and − 22.0 ‰ for $\delta^{18}O$, while rain analyses provide ranges between − 18.7 and − 62.6 ‰ for $\delta^{2}H$ and between − 9.2 and − 9.5 ‰ for $\delta^{18}O$. Spring water isotopic analyses give intermediate values between snow and rainfall, $\delta^{2}H$ from − 61.9 to − 64.2 ‰ and $\delta^{18}O$ from − 9.2 and − 9.5 ‰, and suggest that spring water is a mix between them, with rainfall water being the main component.

Taking advantage of measurements with higher fre-quency (Fig. 11a), the fill and spill hypothesis was applied to FCL using previously collected *Q* data (Deiana et al. 2017). In Fig. 11b, each point in the *R–V* plane is related to a specific subsurface saturation condition. Point *A* has the highest ratio between V and R and corresponds to the highest *Q* value recorded in March (Fig. 11a), when the subsurface undulations are probably completely filled with water. Conversely, point B has the lowest *V/R* value and corresponds to low *Q* values recorded in June, when the subsurface undulations are either partially saturated or dry. According to what was stated in paragraph 3.3, line m passes through the origin of the *V–R* plane and through point A, while line m is parallel to n, passes through point B and the R axis at point I. The value I indicates the mini-mum amount of R needed to increase V in the saturation condition at the end of May/beginning of June 2015.

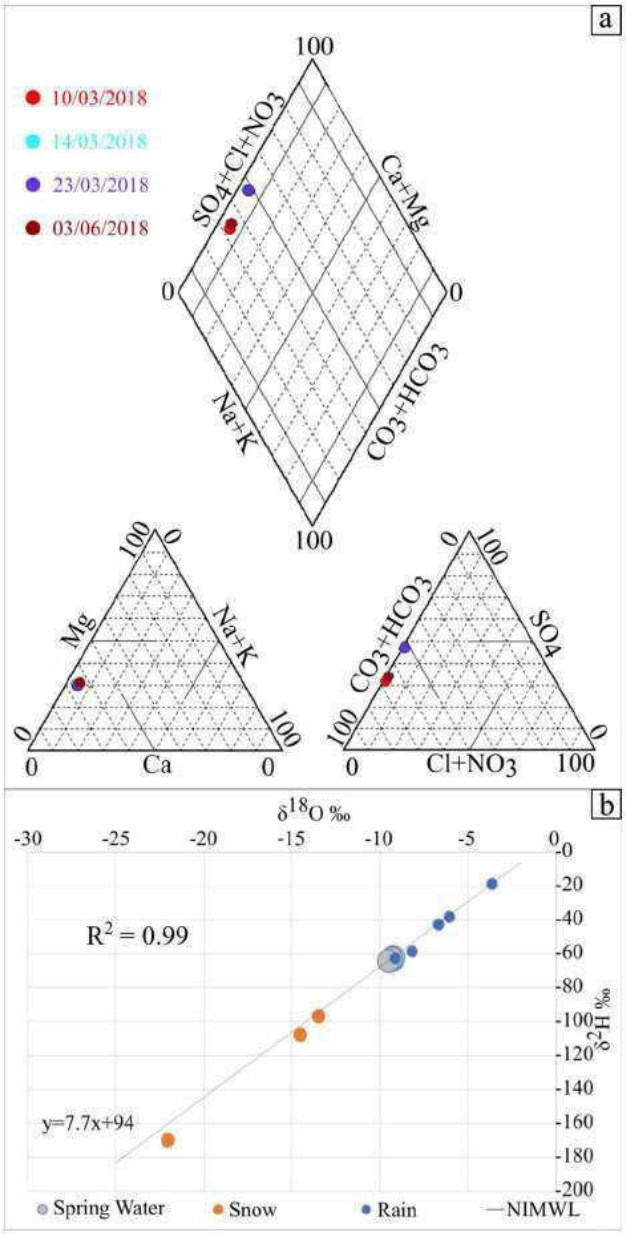

Fig. 10 Piper diagram (**a**) and results of the isotope analyses (**b**) showing groundwater flow type and origin

Discussion

Considering that the estimated maximum depth of the landslide is between 30 and 40 m in the area where S2 is located (Conti and Tosatti 1994) and that both the seismic profiles approximately show a two-layer structure, the interface between the two layers is interpreted as the sliding surface (marked with the red dashed line in Figs. 8a and b). The low velocity values above the interface and the morphology of the topographic surface suggest that the shallow layer consists of fractured calcarenite formation characterised by

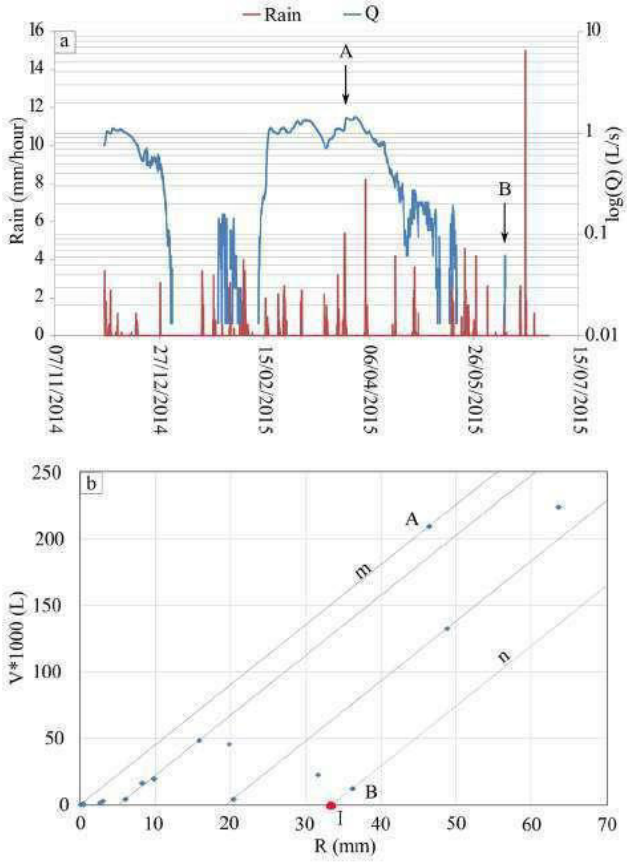

Fig. 11 Q monitored at the spring (blue line) and rainfalls (red bars) (**a**). Application of the fill and spill hypothesis to FCL (**b**). A and B indicate peaks with the highest and the lowest ratio between the vol-ume thatflowed out of the spring (V) and volume of the rain event (R), respectively. The value I represents the minimum amount of recharge water needed to increase V. Line m indicates the relation between V and R when undulations are completely filled. Line n indicates the relation between V and R when the saturation condition is equal to the one during event B

coarse incoherent gravel and rock blocks. The high Vp of the deeper layer can be associated with the P-wave veloc-ity of the bedrock underneath the landslide, i.e. a compact clayey marl formation (Telford et al. 1990). The geoelectri-cal investigation supports the interpretation of the seismic refraction results as the identified shallow high-resistivity values indicate a weathered debris-like medium, while the deeper low-resistivity values can be associated with a con-ductive pelitic bedrock. It can be noticed that the resistivity decreases in the shallow layer from 110 m to the end of S2 (Fig. 8c), while the seismic section has low velocity values in the same area (Fig. 8b). Here, clayey soil with gravel and block debris was observed at the surface, probably having poor mechanical properties (i.e. low Vp) and, at the same time, higher conductivity.

In general, the irregular geometry of the interface between the shallow high-permeability layer and the deeper low-permeability one can promote the storage of groundwater and supports the application of the FSH to develop a thorough hydrogeological conceptual model of FCL defining the groundwater flow and the landslide satu-ration degree over the hydrogeological year. The obtained results (Fig. 10b) suggest two different circulation mecha-nisms: groundwater can directly flow from the recharge area to the spring, or, alternatively, the recharge water cannot directly flow to the spring and the recharge peak is delayed, as suggested by other authors in different hydro-geological contexts (Tromp-Van Meerveld and McDonnell 2006; Wagner et al. 2020). In other words, according to the initial saturation degree of the FCL landslide, subsur-face water can reach the spring along different paths and with different timings, confirming the presence of under-ground undulations where water can be stored. When the undulations are partially saturated and precipitations are weak and rare, the recharge water is stored into the land-slide without any increase in Q observed at the spring. On the contrary, when undulations are partially saturated and rainfalls are intense and/or long-lasting, water can fill up the undulations and flow out causing an increase in Q observed at the spring. Accordingly, until the recharge water fills up the depressions, V is null and R increases, while when water flows out of the undulations, V increases linearly with R.

Assuming that recharge water is characterised by low salinity (Deiana et al. 2020), the water flowing through the landslide body has different ion concentrations depend-ing on the encountered lithologies. Accordingly, three groundwater flows with different features depending on their hydro-chemical composition have been identified. There is a superficial flow (SF) in case of intense and prolonged rainfalls and/or when the slope is highly satu-rated. SF has high carbonate concentration and is actually related to water mainly flowing near the surface through the calcarenite slab and the shallow debris layer identi-fied by the geophysical surveys. Thanks to analyses on samples gathered when rainfalls are rare, a sulphate-rich deep flow (DF) related to water infiltrating at depth and reaching the pelitic formation was identified (Deiana et al. 2016; Marc et al. 2017). This result indicates that water infiltrating into the landslide body does not entirely travel through the shallow layer, but it can reach the sliding sur-face, where it is stored into the undulations and enriches in sulphate, then partially flows out and slowly travels to the spring. Both shallow and deep water circulations can be active when Q is maximum. In such a case, SF and DF mix together in a mixed flow (MF) with high concentration of both anions.

Through monitoring, it was possible to identify four stages that relate landslide saturation to the recharge water provided by precipitations (Fig. 12):

- Stage 1 usually occurs in the wet autumn season and starts with significant rainfall events that recharge the aquifer and reactivate the groundwater flow together with the outflow from the spring. When subsurface undulations are saturated, additional rainfalls cause an increase in both Q and EC, with the latter increasing because of the hydrogeological phenomenon known as pistoning (Tommasone et al. 2011), i.e. the infiltrating water causes the sulphate-rich stored water to flow out of the undulations.
- Stage 2 features intense and lasting precipitation events usually occurring in spring time, when the landslide body is already almost saturated because it has been previously recharged. Accordingly, Q values recorded at the spring are maximum since subsurface undulations are completely water filled, and EC values suggest the presence of an MF resulting from the pistoning effect at depth together with the high saturation of the landslide body.
- Stage 3 starts with the summer time and thus features weak and rare precipitation events. Significant evapotranspiration causes the gradual decrease of Q value and the increase of EC. Rare rainfalls usually trigger SF that produces dilution effect and an increase in carbonate concentration. Very rarely, the recharge water infiltrates at depth and fills the undulations, reactivating the DF and causing a gradual increase of sulphate concentration, until it reaches the maximum value at stage 4.
- Stage 4 occurs during the warmest months, when the landslide saturation is the lowest, precipitations are very rare and evapotranspiration is the highest. Q tends to zero because the shallow layer is dry and the pelitic layer depletes the previously stored water. EC has a high value because water slowly flows only on the slip surface. The application of FSH shows that water infiltrating into the mass movement is effectively stored in subsurface depressions associated with the irregular geometry of the slip surface. However, the slope morphology at the surface suggests the presence of buried rock blocks that can also cre-ate subsurface geometries where water could be temporarily stored on top of the blocks themselves. Unfortunately, geo-physical surveys could not identify subsurface calcarenite blocks because of low resolution. On the other hand, geo-chemical analysis could support this speculative hypothesis (e.g., see peak of carbonate ion concentration after some rainfalls in April 2018; Fig. 9g, i).

Figure 13 depicts a tentative connection between FCL kinematics and subsurface water circulation. It is well known that high saturation is one of the most common landslide-triggering factors, because it increases pore water pressure and causes the shear resistance along the sliding surface to drop. Point A identified in Fig. 11 falls within the wet season in 2015, when saturation is high and the hydraulic response of the landslide body to precipitations is important (Q 1.5 L/s). The Q values in March 2018 are higher than those recorded in 2015 (Q 4.5 L/s, Fig. 13a), suggesting a high saturation of the landslide body and, possibly, underground undulations completely filled with water. This event coin-cides with stage 2 of the proposed hydrogeological model (Fig. 12). InSAR results in terms of average velocity of the reflectors selected in Fig. 2a, b also highlights an increase in the instability of FCL (Fig. 13b). The marked decrease in $\delta^{18}O$ from − 9.19 to − 9.56 ‰ (Fig. 13c) observed thanks to spring water isotopes analyses suggests that water infil-tration due to snowmelt right before the occurrence of the Q peak (Fig. 9i) may have increased the saturation and the instability of FCL.

Conclusion

Based on a multidisciplinary approach involving non-invasive techniques from different disciplines, a hydrogeologi-cal conceptual model was developed and the evolution of the complex Fontana Cornia landslide was evaluated. Geophysical data showed that the landslide has a curvilinear

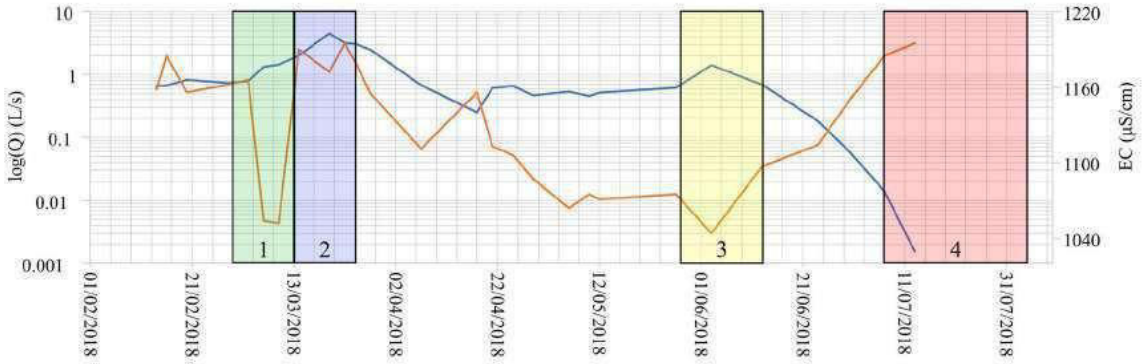

Fig. 12 Spring discharge (Q) and electrical conductivity (EC) curves during different hydrogeological stages, namely recharge (1), wet (2), dis-charge (3) and dry periods (4), indicated by coloured rectangles

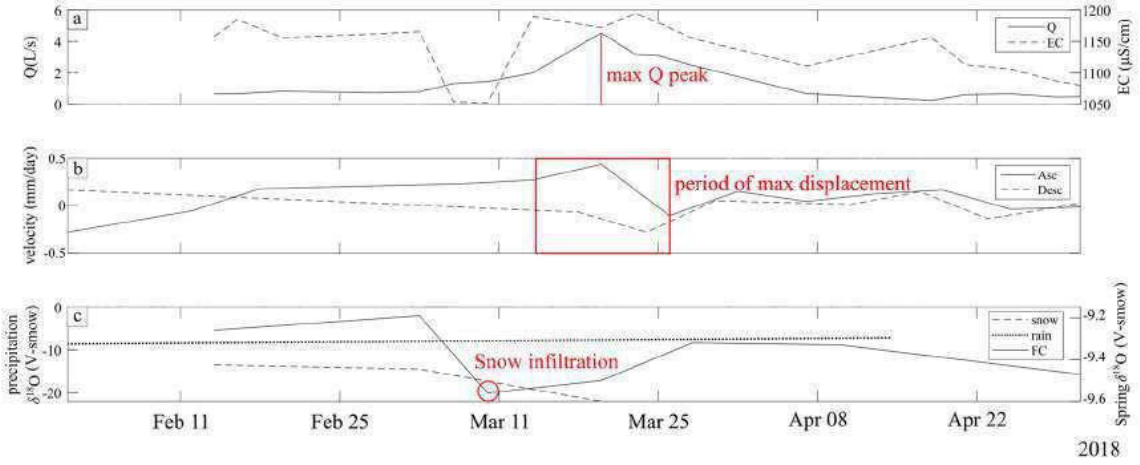

Fig. 13 Comparison between hydrological (**a**), remote sensing (**b**) and isotopic monitoring datasets (**c**). The maximum discharge peak (*Q*) in (**a**) is marked with the vertical red line and matches the maxi-mum displacement enclosed in the red square in (**b**). The low spring water value for $\delta^{18}O$ in the red circle in (**c**) suggests that the snow infiltrated into the subsurface right before the maximum displacement and the maximum discharge

sliding surface dividing the shallow calcarenite debris layer from the deeper pelitic bedrock. The geometry of the interface involves undulations in which water can be stored and supports the application of the fill and spill hypoth-esis. The hydrogeological monitoring of precipitations and of the spring water discharge allows defining the satura-tion condition of the subsurface over time. Using the joint interpretation of the hydrogeological, hydro-chemical and geophysical outcomes according to the FSH, a hydrogeo-logical conceptual model was defined. The model involves four specific hydrologic stages. Each stage features a main groundwater flow through the landslide body, namely the shallow, deep, and mixed flows.

The developed hydrogeological model allows an under-standing of the groundwater processes that may explain the behaviour of the landslide in terms of displacements. In more detail, the isotope analyses, displacement moni-toring, and hydrogeological measurements confirm that periods with significant precipitations and snowmelt can cause an increase in landslide saturation that in turn trig-gers larger displacements. Conversely, the landslide slowly moves at a steady rate during periods with limited recharge water.

Author contributions All authors contributed to the study conception and design. Material preparation, data collection and analysis were performed by AA, DA, MM, GC, BB, GW and FR. The first draft of the manuscript was written by AA and DA and all authors commented on previous versions of the manuscript. All authors read and approved the final manuscript.

Funding The authors declare that no funds, grants, or other support were received during the preparation of this manuscript.

Declarations

Conflict of interest The authors have no relevant financial or non-fi-nancial interests to disclose.

References

Aguzzoli A, Zanzi L, Arosio D (2021) Seismic noise azimuthal spectral ratios to monitor landslide kinematics. In 27th European Meeting of Environmental and Engineering Geophysics, Aug 2021, Volume 2021, p.1 – 5. European Association of Geoscientists & Engineers. https://doi.org/10.3997/2214-4609.202120213

Arosio D, Corsini A, Giusti R, Zanzi L (2017) Seismic noise measurements on unstable rock blocks: the case of bismantova rock cliff. In: Advancing culture of living with landslides. https://doi.org/10.1007/978-3-319-53487-9_37

Arosio D, Longoni L, Papini M, Bièvre G, Zanzi L (2019) Geological and geophysical investigations to analyse a lateral spread-ing phenomenon: the case study of Torrioni di Rialba, northern Italy. Landslides 16(7):1257–1271. https :// doi.org/ 10.1007/s10346-019-01176-w

Bayer B, Simoni A, Mulas M, Corsini A, Schmidt D (2018) Deformation responses of slow-moving landslides to seasonal rainfall in the Northern Apennines, measured by InSAR. Geomorphology 308:293–306. https://doi.org/10.1016/j.geomorph.2018.02.020

Berman ESF, Gupta M, Gabrielli C, Garland T, McDonnell JJ (2009) High-frequency field-deployable isotope analyzer for hydrological applications. Water Resour Res 45:1–7. https ://doi.org/10.1029/2009WR008265

Binley A, Kemna A (2005) DC resistivity and induced polarization methods. In: Rubin Y, Hubbard SS (eds) Hydrogeophysics. Water Science and Technology Library, vol 50. Springer, Dordrecht, pp 129–156. https://doi.org/10.1007/1-4020-3102-5_5

Birk S, Liedl R, Sauter M (2004) Identification of localised recharge and conduit flow by combined analysis of hydraulic and physico-chemical spring responses (Urenbrunnen, SW-Germany). J Hydrol 286:179–193. https :// doi. org/ 10. 1016/j. jhydrol.2003.09.007

Bogaard TA, Greco R (2016) Landslide hydrology: from hydrology to pore pressure. Wiley Interdiscip Rev Water 3:439–459. https :// doi.org/10.1002/wat2.1126

Borgatti L, Tosatti G (2010) Slope Instability Processes Affecting the Pietra Di Bismantova Geosite (Northern Apennines, Italy). Geoheritage 2:155–168. https :// doi. org/ 10. 1007/ s12371- 010- 0023-8

Brkić Ž, Kuhta M, Hunjak T (2018) Groundwater flow mechanism in the well-developed karst aquifer system in the western Croa-tia: insights from spring discharge and water isotopes. CATENA. https://doi.org/10.1016/j.catena.2017.10.011

Cappa F, Guglielmi Y, Soukatchoff VM, Mudry J, Bertrand C, Charmoille A (2004) Hydromechanical modeling of a large moving rock slope inferred from slope levelling coupled to spring long-term hydrochemical monitoring: example of the La Clapière land-slide (Southern Alps, France). J Hydrol. https://doi.org/10.1016/j.jhydrol.2003.12.013

Conti S, Tosatti G (1994) Caratteristiche geologico-strutturali della Pietra di Bismantova e fenomeni franosi connessi. Quad Geol Appl 1:25–43

Corsini A, Bonacini F, Mulas M, Ronchetti F, Monni A, Pignone S, Primerano S, Bertolini G, Caputo G, Truffelli G, Benini A, Berti M (2015a) A portable continuous GPS array used as rapid deployment monitoring system during landslide emergencies in Emilia Romagna. Rendiconti Online Societa Geologica Italiana 35:89–91. https://doi.org/10.3301/ROL.2015.71

Corsini A, Bonacini F, Mulas M, Petitta M, Ronchetti F, Truffelli G (2015b) Long-term continuous monitoring of a deep-seated compound rock slide in the Northern Apennines (Italy), Engineering Geology for Society and Territory—volume 2: landslide pro-cesses. https://doi.org/10.1007/978-3-319-09057-3_235

Corsini A, Bonacini F, Deiana M, Giusti R (2016) A wireless crackmeters network for the analysis of rock falls at the Pietra di Bis-mantova natural heritage site (Northern Apennines, Italy) A wireless crackmeters network for the analysis of rock falls at the Pietra di Bismantova natural heritage site. https://doi.org/10.1201/b21520-78

Deiana M, Cervi F, Bertrand C, Ronchetti F (2016) Hydrogeological investigation of Pietra di Bismantova slab and surrounding slope deposits (northern Apennines, Italy). Rend Online Soc Geol It 41:135–138. https://doi.org/10.3301/ROL.2016.112

Deiana M, Mussi M, Ronchetti F (2017) Discharge and environmental isotope behaviours of adjacent fractured and porous aquifers. Environ Earth Sci. https://doi.org/10.1007/s12665-017-6897-xDeiana M, Cervi F, Pennisi M, Mussi M, Bertrand C, Tazioli A, Cors-ini A, Ronchetti F (2018) Chemical and isotopic investigations (δ 18 O, δ 2 H, 3 H, 87 Sr/86 Sr) to define groundwater pro-cesses occurring in a deep-seated landslide in flysch. Hydrogeol J 26(8):2669–2691

Deiana M, Mussi M, Pennisi M, Boccolari M, Corsini A, Ronchetti F (2020) Contribution of water geochemistry and isotopes (δ 18 O, δ 2 H, 3 H, 87 Sr/86 Sr and δ 11 B) to the study of groundwater flow properties and underlying bedrock structures of a deep landslide. Environ Earth Sci 79(1):30

Del Gaudio V, Wasowski J, Muscillo S (2013) New developments in ambient noise analysis to characterise the seismic response of landslide-prone slopes. Nat Hazard 13:2075–2087. https://doi.org/10.5194/nhess-13-2075-2013

Delgado J, Vicente F, García-Tortosa F, Alfaro P, Estévez A, Lopez Sanchez JM, Tomás R, Mallorquí JJ (2011) A deep seated com-pound rotational rock slide and rock survey in SE Spain: structural control and DInSAR monitoring. Geomorphology 129:252–262. https://doi.org/10.1016/j.geomorph.2011.02.019

Epstein S, Mayeda T (1953) Variation of O18 content of waters from natural sources. Geochim Cosmochim Acta. https://doi.org/10.1016/0016-7037(53)90051-9

Friedel S (2003) Resolution, stability and efficiency of resistivity tomography estimated from a generalized inverse approach. Geophys J Int 153:305–316

Gargini A, Vincenzi V, Piccinini L, Zuppi GM, Canuti P (2008) Groundwater flow systems in turbidites of the Northern Apen-nines (Italy): natural discharge and high speed railway tunnel drainage. Hydrogeol J 16:1577–1599. https://doi.org/10.1007/s10040-008-0352-8

Glynn PD, Plummer LN (2005) Geochemistry and the understanding of ground-water systems. Hydrogeol J 13:263–287. https://doi.org/10.1007/s10040-004-0429-y

Hooper A, Segall P, Zebker H (2007) Persistent scatterer interferometric synthetic aperture radar for crustal deformation analysis, with application to Volcán Alcedo. Galápagos 112:1–21. https://doi.org/10.1029/2006JB004763

Iasio C, Novali F, Corsini A, Mulas M, Branzanti M, Benedetti E, Giannico C, Tamburini A, Mair V (2012) COSMO SkyMed high frequency - high resolution monitoring of an alpine slow landslide, corvara in Badia, Northern Italy. In Proceedings of the IEEE International Geoscience and Remote Sensing Symposium; IEEE, 2012; pp. 7577–7580. https :// doi. org/ 10. 1109/IGARSS.2012.6351908

Ivanov V, Arosio D, Tresoldi G, Hojat A, Zanzi L, Papini M, Longoni L (2020) Investigation on the role of water for the stability of shallow landslides-insights from experimental tests. Water (Swit-zerland) 12:1203. https://doi.org/10.3390/W12041203

Jongmans D, Garambois S (2007) Geophysical investigation of landslides: a review. Bull Soc Geol Fr 178:101–112. https://doi.org/10.2113/gssgfbull.178.2.101

Krzeminska DM, Bogaard TA, Van Asch TWJ, Van Beek LPH (2012) A conceptual model of the hydrological influence of fissures on landslide activity. Hydrol Earth Syst Sci 16:1561–1576. https :// doi.org/10.5194/hess-16-1561-2012

Liu X, Zhao C, Zhang Q, Peng J, Zhu W, Lu Z (2018) Multi-temporal loess landslide inventory mapping with C-, X- and L-band SAR datasets—a case study of heifangtai loess landslides, China. Remote Sens 10:1756. https://doi.org/10.3390/rs10111756

Loke MH, Acworth I, Dahlin T (2003) A comparison of smooth and blocky inversion methods in 2D electrical imaging surveys. Explor Geophys 34:182–187. https://doi.org/10.1071/EG03182

Longinelli A, Selmo E (2003) Isotopic composition of precipitation in Italy: a first overall map. J Hydrol 270:75–88

Longoni L, Arosio D, Scaioni M, Papini M, Zanzi L, Roncella R, Brambilla D (2012) Surface and subsurface non-invasive investi-gations to improve the characterization of a fractured rock mass. J Geophys Eng 9:461–472

Mainsant G, Larose E, Brnnimann C, Jongmans D, Michoud C, Jaboyedoff M (2012) Ambient seismic noise monitoring of a clay landslide: Toward failure prediction. J Geophys Res Earth Surf 117:1–12. https://doi.org/10.1029/2011JF002159

Maloszewski P, Rauert W, Trimborn P, Herrmann A, Rau R (1992) Isotope hydrological study of mean transit times in an alpine basin (Wimbachtal, Germany). J Hydrol 140:343–360. https://doi.org/10.1016/0022-1694(92)90247-S

Marc V, Bertrand C, Malet JP, Carry N, Simler R, Cervi F (2017) Groundwater—surface waters interactions at slope and catchment scales: implications for landsliding in clay-rich slopes. Hydrol Process 31(2):364–381

Meric O, Garambois S, Jongmans D, Wathelet M, Chatelain JL, Vengeon JM (2005) Application of geophysical methods for the investigation of the large gravitational mass movement of Séchili-enne, France. Can Geotech J 42:1105–1115. https ://doi.org/10.1139/t05-034

Mulas M, Marnas M, Ciccarese G, Corsini A (2020) Sinusoidal wave fit indexing of irreversible displace- ments for crackmeters

monitoring of rockfall areas: test at Pietra di Bismantova (Northern Apennines, Italy) 231–240. https ://doi.org/10.1007/s10346-019-01248-x

Papani G, De Nardo MT, Bettelli G, Rio D, Tellini C, Vernia L, Cibin U (2002) Note Illustrative della Carta Geologica d'Italia alla scala 1: 50.000, Foglio 218, Castelnuovo ne'Monti. EL. CA. Firenze, Servizio Geologico d'Italia—Regione Emilia Romagna.

Ronchetti F, Piccinini L, Deiana M, Ciccarese G, Vincenzi V, Aguzzoli A, Malavasi G, Fabbri P, Corsini A (2020) Tracer test to assess flow and transport parameters of an earth slide: The Montecagno landslide case study (Italy). Eng Geol 275:105749. https://doi.org/10.1016/j.enggeo.2020.105749

Roy A, Apparao A (1971) Depth of investigation in direct current methods. Geophysics 36(5):943–959

Rücker C, Günther T, Wagner F (2016) pyGIMLi—an open source python library for inversion and modelling in geophysics. In 78th EAGE Conference and Exhibition 2016, European Association of Geoscientists & Engineers.

Sheehan JR, Doll WE, Mandell WA (2005) An evaluation of methods and available software for seismic refraction tomography analysis. J Environ Eng Geophys 10(1):21–34

Sidle RC, Greco R, Bogaard T (2019) Overview of landslide hydrology. Water (Switzerland) 11:11–13. https://doi.org/10.3390/w11010148

Taruselli M, Aguzzoli A, Zanzi L, Arosio D (2020) Monitoring Ca Lita Landslide by Means of the Ambient Seismic Noise. In 3rd Asia Pacific Meeting on Near Surface Geoscience & Engineering, Nov 2020, Volume 2020, p.1 – 5. European Association of Geoscientists & Engineers. https://doi.org/10.3997/2214-4609.202071088

Tazioli A, Conversini P, Peccerillo A (2012) Hydrogeological and geochemical characterisation of the Rock of Orvieto. Environ Earth Sci 66:55–65. https://doi.org/10.1007/s12665-011-1206-6

Tazioli A, Cervi F, Doveri M, Mussi M, Deiana M, Ronchetti F (2019) Estimating the isotopic altitude gradient for hydrogeological studies in mountainous areas: are the low-yield springs suitable? Insights from the northern Apennines of Italy. Water 11(9):1764

Telford WM, Geldart LP, Sheriff RE (1990) Applied geophysics, 2nd edn. Cambridge University Press, Cambridge. https://doi.org/10.1017/CBO9781139167932

Thiebes B, Tomelleri E, Mejia-Aguilar A, Rabanser M, Schlögel R, Mulas M, Corsini A (2016) Assessment of the 2006 to 2015 Corvara landslide evolution using a UAV-derived DSM and orthophoto. Landslides and engineered slopes. Experience Theory Practice 3:1897–1902. https://doi.org/10.1201/b21520-237

Tommasone FP, De Francesco S, Cuoco E, Verrengia G, Santoro D, Tedesco D (2011) Radon hazard in shallow groundwaters II: dry season fracture drainage and alluvial fan upwelling. Sci Total Environ. https://doi.org/10.1016/j.scitotenv.2011.05.039

Tromp-van Meerveld HJ, McDonnell JJ (2006) Threshold relations in subsurface stormflow: 2. The fill and spill hypothesis. Water Resour Res 42(2):W02411. https :// doi. org/ 10. 1029/ 2004WR003800

Vallet A, Bertrand C, Mudry J, Bogaard T, Fabbri O, Baudement C, Régent B (2015) Contribution of time-related environmental trac-ing combined with tracer tests for characterization of a groundwa-ter conceptual model: a case study at the Séchilienne landslide, western Alps (France). Hydrogeol J 23(8):1761–1779

Wagner T, Brodazc A, Krainer K, Winkler G (2020) Active rock glaciers as shallow groundwater reservoirs, Austrian Alps. Grundwasser. https://doi.org/10.1007/s00767-020-00455-xWinkler G, Wagner T, Pauritsch M, Birk S, Kellerer-Pirklbauer A, Benischke R, Leis A, Morawetz R, Schreilechner MG, Hergarten S (2016) Identification and assessment of groundwater flow and storage components of the relict Schöneben Rock Glacier, Niedere Tauern Range, Eastern Alps (Austria). Hydrogeol J 24:937–953. https://doi.org/10.1007/s10040-015-1348-9

Zhang Z, Arosio D, Hojat A, Zanzi L (2020) Tomographic experiments for defining the 3D velocity model of an unstable rock slope to support microseismic event interpretation. Geosciences 10(9):327. https://doi.org/10.3390/geosciences10090327